Generation of quasi-monoenergetic protons from thin multi-ion foils by a combination of laser radiation pressure acceleration and shielded Coulomb repulsion

2013 New J. Phys. 15 025026

(http://iopscience.iop.org/1367-2630/15/2/025026)

New Journal of Physics
The open access journal for physics

Generation of quasi-monoenergetic protons from thin multi-ion foils by a combination of laser radiation pressure acceleration and shielded Coulomb repulsion

Tung-Chang Liu[1,6], Xi Shao[1], Chuan-Sheng Liu[1], Minqing He[1], Bengt Eliasson[1,2], Vipin Tripathi[1,3], Jao-Jang Su[1], Jyhpyng Wang[4,5] and Shih-Hung Chen[5]

[1] Department of Physics, University of Maryland, College Park, MD 20742, USA
[2] Institute for Theoretical Physics, Ruhr-University Bochum, D-44780 Bochum, Germany
[3] Department of Physics, Indian Institute of Technology, New Delhi 110016, India
[4] Institute of Atomic and Molecular Sciences, Academia Sinica, Taipei 10617, Taiwan
[5] Department of Physics, National Central University, Taoyuan 32001, Taiwan
E-mail: tcliu@umd.edu

New Journal of Physics **15** (2013) 025026 (16pp)
Received 24 July 2012
Published 19 February 2013
Online at http://www.njp.org/
doi:10.1088/1367-2630/15/2/025026

Abstract. We study theoretically and numerically the acceleration of protons by a combination of laser radiation pressure acceleration and Coulomb repulsion of carbon ions in a multi-ion thin foil made of carbon and hydrogen. The carbon layer helps to delay the proton layer from disruption due to the Rayleigh–Taylor instability, to maintain the quasi-monoenergetic proton layer and to accelerate it by the electron-shielded Coulomb repulsion for much longer duration than the acceleration time using single-ion hydrogen foils. Particle-in-cell simulations with a normalized peak laser amplitude of $a_0 = 5$ show a resulting quasi-monoenergetic proton energy of about 70 MeV with the foil made of 90% carbon and 10% hydrogen, in contrast to 10 MeV using a single-ion hydrogen foil.

[6] Author to whom any correspondence should be addressed.

An analytical model is presented to explain quantitatively the proton energy evolution; this model is in agreement with the simulation results. The energy dependence of the quasi-monoenergetic proton beam on the concentration of carbon and hydrogen is also studied.

Contents

1. Introduction

In recent years, the search for a novel mechanism for the acceleration of monoenergetic protons has gained much interest, in particular for its use in proton cancer therapy, because of its low collateral damage to healthy tissue [1–3]. In proton cancer therapy, monoenergetic proton beams of high quality with fluxes of 10^9–10^{11} particles per second and with a tunable energy of 50–250 MeV are required in order to target the tumor location. A compact laser-driven proton accelerator would be attractive since the electric fields for particle acceleration can reach the order of tens of GV per centimeter, which allows for a significant reduction of the system size [4, 5]. Inspired by the milestone works [6–8] about producing monoenergetic electrons by laser wakefield acceleration [9] and the subsequent works [10, 11] about obtaining quasi-monoenergetic electrons close to 1 GeV, we report in this paper an effective method for laser acceleration of quasi-monoenergetic protons with a modest laser power using multi-ion targets.

In recent years, various mechanisms for the acceleration of protons by laser irradiation on a foil have been actively studied, for example, target normal sheath acceleration (TNSA), radiation pressure acceleration (RPA), shock acceleration, Coulomb explosion, etc. In TNSA [12–20], laser irradiates on a thick target, and protons are accelerated by the sheath electric field created by the hot electrons heated by the laser. The resulting ion energy spectra are broad and only a few protons reach the maximum energy. The RPA scheme, which uses circularly polarized laser irradiating on ultra-thin films for producing quasi-monoenergetic protons, has been actively studied in theory and simulations [21–27] and experiments [28, 29], because it can generate protons with good beam quality and a narrow energy spectrum, suitable for many applications. Marx first proposed the RPA scheme [30, 31] for the acceleration of the solid foil for space application with the laser beam being perfectly reflected without any influence on the inner structure of the foil. However, when the laser beam is intense enough

to ionize the target to form a plasma, many effects, such as shock formation [32–35], hole-boring (a phase while the laser beam compresses and drills a hole into the foil prior to the RPA phase [12, 36, 37]) and various instabilities, are observed to destroy the integrity of the foil. For laser acceleration of thin plasma in one dimension, a stable double layer can be formed with both electrons and protons trapped in the potential well [25], and the analysis of RPA can be found in the appendix.

However, it was shown by two-dimensional (2D) particle-in-cell (PIC) simulations that the Rayleigh–Taylor instability (RTI) can limit the ion acceleration achieved by RPA and broaden the proton beam's energy spectrum [24, 26, 38–41]. This is one of the most important instabilities arising when a thin plasma foil is accelerated by the laser radiation pressure. It puts a limit on the time a foil can be accelerated before it becomes transparent to the laser light and loses its monoenergetic properties. For RPA of a thin-foil target of one species, the energy scaling study with PIC simulations [42] indicates that a high-power (2–3 pW) laser is needed to obtain around 200 MeV quasi-monoenergetic protons with an energy spread within 20% of the peak flux energy. Several studies for understanding and overcoming the unfavorable RTI effect have been performed [39, 41, 43–45], and this is still a topic of ongoing research.

We show in this paper that it is feasible to generate a 60 MeV proton beam with a modest laser power of 70 TW by combining the RPA and shielded Coulomb repulsion (SCR), using a multi-ion foil made of majority carbon (90%) and minority hydrogen (10%). This combination can significantly extend the duration of acceleration for the quasi-monoenergetic protons, and hence a proton beam with much higher energy can be produced with the same laser power. The carbon layer delays the disruption of proton layer due to the RTI significantly while accelerating the proton layer and maintaining its integrity. Earlier work [46] on using the Coulomb repulsion force between ions in acceleration used a laser beam with a large intensity to sweep out the electron and to instantaneously accelerate protons by direct Coulomb explosion. In this work, we instead applied a laser beam with a modest power and observed that the acceleration is stable for a long time while the repulsive force is partially shielded by the electrons. There have been a few studies of the interactions between laser and multi-species targets [45, 47, 48] that indicate a similar proton acceleration. However, the physics of acceleration and scaling of achievable proton energy is not well understood. In particular, Qiao *et al* [48] proposed late stage proton acceleration due to leaky laser radiation, whose physics is different from what we consider here, the combined RPA and SCR mechanism. In this paper, we present the scaling of the proton energy with respect to the initial carbon/hydrogen concentration ratios and the initial density of the foil by using 2D PIC simulations. Finally, we present a theoretical model of the proton acceleration by SCR that agrees well with simulation results.

2. Generation of quasi-monoenergetic protons by radiation pressure acceleration and shielded Coulomb repulsion

In this work, we employ 2D PIC simulations to study the production of quasi-monoenergetic protons generated by a combination of RPA and SCR from a multi-ion foil consisting of carbon and hydrogen. The simulation domain is $-30 \leqslant x/\lambda_L \leqslant 70$, $-15 \leqslant y/\lambda_L \leqslant 15$ and is divided into 100 grids per wavelength. The field boundary conditions are absorbing at the $\pm y$ and $+x$ boundaries, and the laser beam is injected at the $-x$ boundary. Absorbing boundary conditions are used for the particles at all boundaries. The foil is initially located at $0 \leqslant x \leqslant l_0$ with $l_0 = 0.2\lambda_L$ being the foil thickness, and is resolved by 49 quasi-particles of each species per grid.

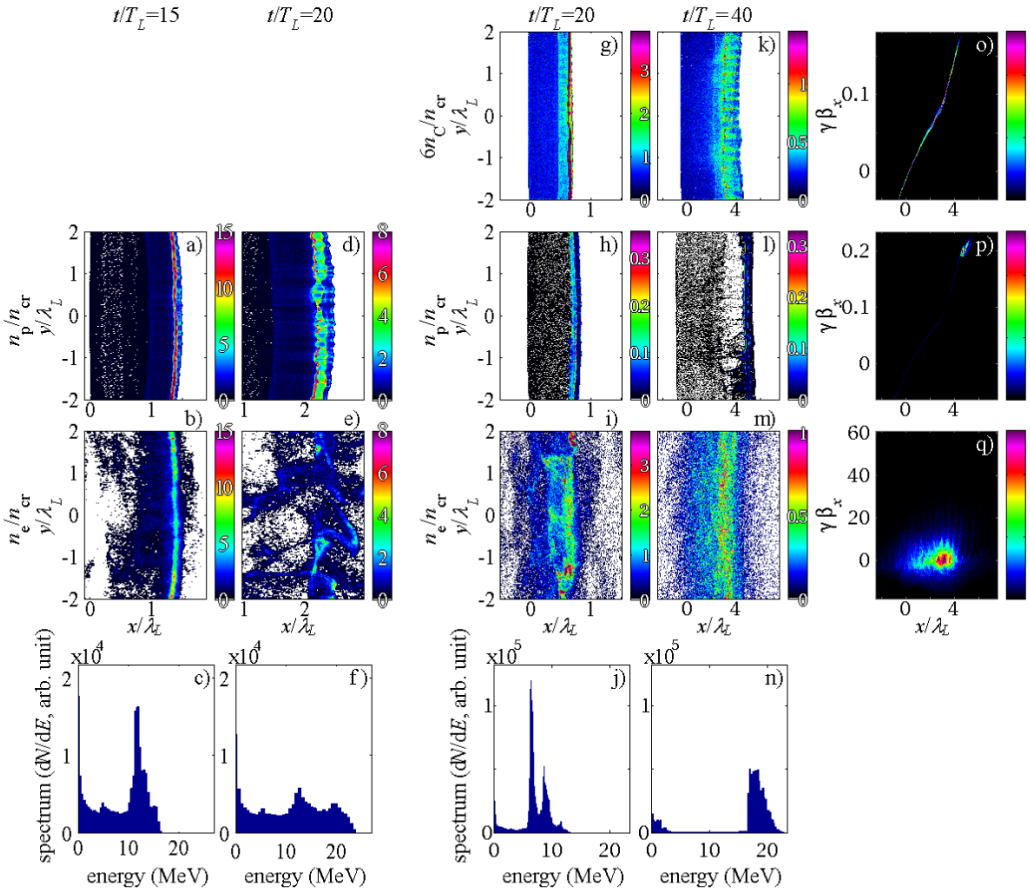

Figure 1. 2D PIC simulation results showing the evolution of a single-ion foil and a multi-ion foil accelerated by a circularly polarized laser. The first three rows from the top are the density maps of the carbon ions, protons and electrons, respectively. The fourth row is the proton energy histogram within a window of $|y| < \lambda_L$ and covering the entire simulation range in x. The first and second columns represent the times when electron layers become transparent and post-transparent, respectively, in the acceleration of a single-ion foil. The third and fourth columns represent the same condition in the acceleration of a multi-ion foil. The fifth column is the phase space of the fourth column with arbitrary units in the colorbars, which shows the trapping of the protons while the velocities of the carbon ions are widely spread. The color of zero value in this column is set as black to emphasize the difference.

The time step is $0.0067T_L$, with $T_L = 3.33$ fs, corresponding to $\lambda_L = 1\,\mu$m. The amplitude of the incident circularly polarized laser has a Gaussian profile in the transverse direction with the spot size being $16\lambda_L$ in diameter and a time profile of $3\lambda_L$ Gaussian rising time and a continuous waveform thereafter.

Figure 1 presents a comparison between the evolution of foils consisting of (i) 90% carbon and 10% hydrogen and (ii) pure hydrogen, accelerated by a circularly polarized laser beam of

normalized amplitude $a_0 = \max(a_y) = \max(a_z) = 5$, corresponding to $I_0 = \varepsilon_0 m_e^2 c^3 \omega_L^2 a_0^2 / e^2 = 3.4 \times 10^{19}\,\mathrm{W\,cm\,s^{-2}}$. The initial electron density is $n_{e0} = 8.3 n_{cr} = 9.25 \times 10^{21}\,\mathrm{cm^{-3}}$, which satisfies the optimal thickness condition [25] of the RPA of a single-species foil. The comparison between the single- and multi-species foil cases shows clearly that the acceleration time for the multi-species foil is significantly longer, and the obtainable proton energy is higher. For the RPA of a hydrogen foil, the RTI destroys the electron layer and widens the energy spectrum of the protons within 20 wave periods. During the RPA, once the electron density of the foil falls below the critical value, the laser light can leak through the target and no longer efficiently accelerates the protons. On the other hand, for the acceleration of a multi-ion foil, the mechanism of the acceleration can be divided into two phases. During the RPA phase, while the whole foil is accelerated, the lighter protons with a greater charge-to-mass ratio pass ahead of the heavier carbon ions. The RTI creates transverse density ripples in the carbon and proton layers. When the electron layer becomes underdense due to the RTI, it is no longer pushed by the radiation pressure, and the carbon layer stops from being accelerated, leaving the proton layer ahead. This leads to the SCR phase, where the net electrostatic field from the carbon-electron layer further pushes the proton layer forward and accelerates it to higher energy. After the foil has become transparent to the laser light, the electron layer stabilizes to provide a static electrostatic field, which accelerates the protons and smoothens the transverse density ripples in the proton layer. The protons are now held as a stable layer, boosting the acceleration time to about $200T_L$, which is an improvement of one order of magnitude compared to the RPA of the single-ion proton foil.

The acceleration mechanism is demonstrated quantitatively in figure 2, where the proton layer is continuously accelerated (figure 2(a)) while retaining its monoenergetic property (figure 2(b)) even after the electron layer has become transparent to the laser beam. In contrast, the carbon layer, which acts as the proton layer in acceleration of a single-ion foil, is initially accelerated by RPA until the electrons become underdense owing to the RTI. The acceleration of protons is attributed to the spatial charge distribution, which consists of the electrons in front of the proton layer and the partially shielded carbon layer behind it. Figure 2(c) shows the density distribution within $|y| < \lambda_L$ when the electron density is far below the critical density. Due to the scarce number of the electrons in front of the proton layer, the acceleration from behind (the SCR) is the dominant factor pushing the proton layer forward. To differentiate the contribution of the static electric field behind the proton layer at position x_p to the one ahead of it, the longitudinal electric field due to the charge sources from behind within $|y| < \lambda_L$ by one-dimensional (1D) calculation, E_{xL}, is shown in figure 2(d), along with the electric field computed from the charges both behind and ahead of the foil, E_{xtot}, and the one obtained from the simulation, E_{xsim}. That is,

$$\begin{aligned} E_{xL} &= \tfrac{e}{2\varepsilon_0} \textstyle\int_{-\infty}^{x_p} [6\bar{n}_C(x) - \bar{n}_e(x)]\,\mathrm{d}x, \\ E_{xtot} &= \tfrac{e}{2\varepsilon_0} \textstyle\int_{-\infty}^{\infty} [6\bar{n}_C(x) - \bar{n}_e(x)]\mathrm{sgn}(x_p - x)\,\mathrm{d}x, \\ E_{xsim} &= \bar{E}_x(x = x_p), \end{aligned} \tag{1}$$

where the overbar indicates average taken along the y direction over the range $|y| < \lambda_L$. At a later stage ($t > 80T_L$), we can see that the electric field from the charges behind is the major portion of the total electric field at the position of the proton. The good agreement between the simulation data and the 1D electric field interpretation in figure 2(d) also shows that using the 1D model in computing the equation of motion can relatively simply describe the acceleration scheme quantitatively within acceptable errors, which leads to the argument shown in section 4.

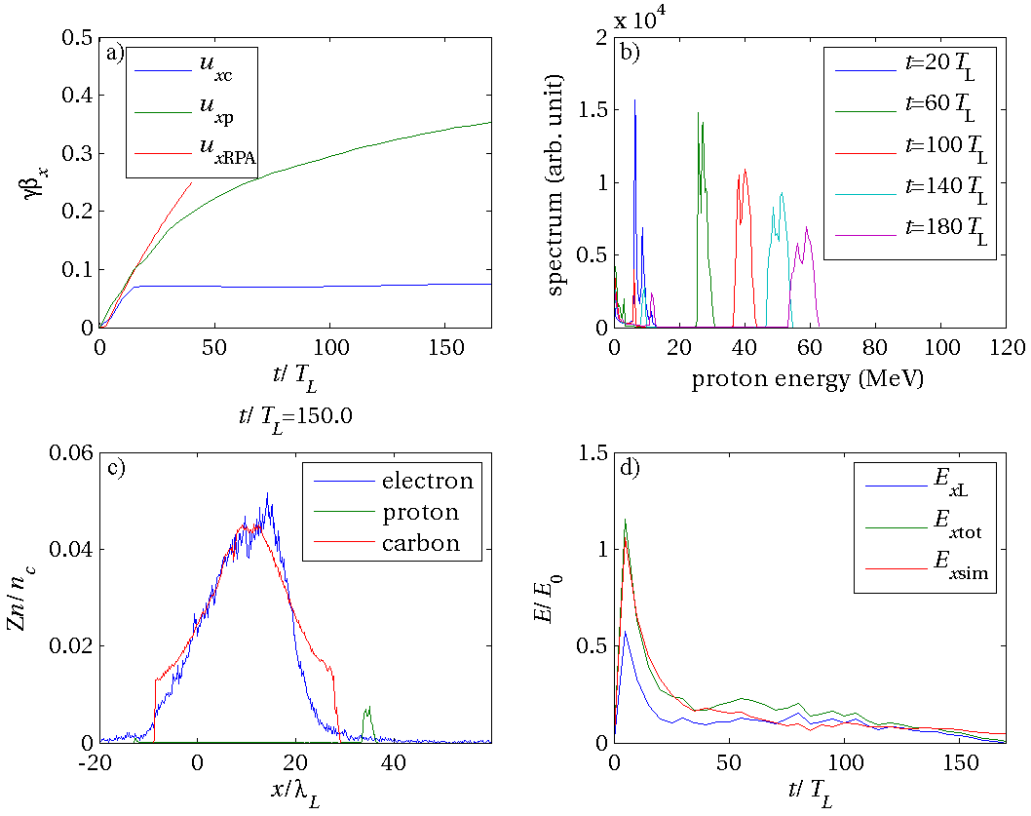

Figure 2. Simulation results with the same input parameters as the multi-ion case shown in figure 1. (a) Time evolution of ion momenta averaged within a window of $|y| < \lambda_L$ and 1D theoretical calculation using equation (A.3). The blue, green and red lines represent the average longitudinal velocities of the carbon ions, protons and the theoretical velocity prediction of the foil as a whole, respectively. (b) The time evolution of proton energy spectra within $|y| < \lambda_L$. (c) The charge density of the charged particles with respect to x at $y = 0$ when $t = 150T_L$. (d) The evolution of the longitudinal electric fields at the position of the proton foil computed from the charges from behind (blue line) and from both behind and ahead (green line), compared with the simulation results (red line).

3. Scaling of the acceleration time and proton monoenergy with carbon concentration

By increasing the percentage of carbon ions, the portion of protons falling behind decreases and the Coulomb repulsion from the carbon ions becomes higher. Therefore, the protons can continue to be accelerated as a monoenergetic layer for a longer time. The obtainable energy is also substantially increased. To explore the relationship between the concentration of carbon and the obtainable energy, we perform a series of simulations increasing the fraction of carbon in the foil with 10% increment, decreasing the fraction of protons accordingly and keeping the initial electron number density as a constant. The result is shown in figure 3. For carbon concentrations lower than 50%, there are two mechanisms dominating the obtainable energy with increasing carbon percentage—reduction of the RPA due to a heavier foil and enhancement of the SCR due to a larger number of carbon ions and less overlapping between the carbon layer and the

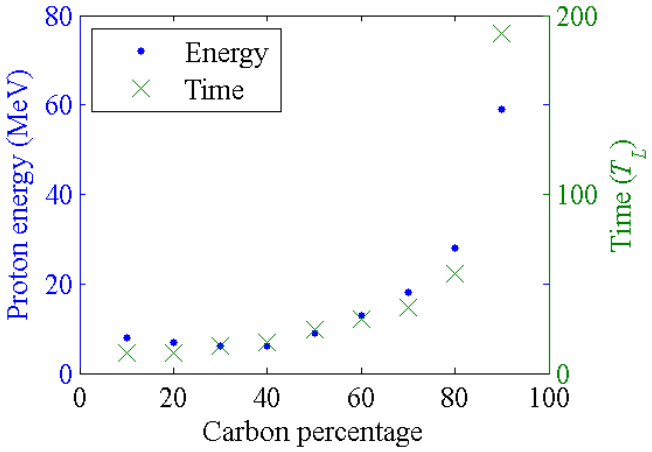

Figure 3. The energy scaling of protons with respect to the carbon concentration in the cases of multi-ion acceleration from 2D PIC simulations. The saturation time t_s is recorded when the maximum of quasi-monoenergy (under the constraint $\Delta\mathcal{E}/\mathcal{E} \leqslant 20\%$) is obtained.

proton layer. The latter factor becomes relatively more significant with increasing carbon concentration, and at 50%, the Coulomb repulsion is large enough to compensate for the reduction of the RPA.

The obtainable energy from the Coulomb force is proportional to the total charge of the carbon layer, leading to a larger electric potential. Increasing the carbon concentration can provide greater repulsive force and energy. It is shown in figure 3 that in the region of small carbon percentage, the obtainable proton monoenergy is slightly decreased with increasing carbon percentage. In this region, the separation of the carbon and proton layers is not significant, so that the repulsion force from the carbon layer is not large enough to enhance the obtainable energy against the reduction of the RPA. For higher carbon concentration, the proton layer is almost totally separated from the carbon ion layer during the RPA phase, and thus maintains monoenergy for a longer time and accelerates more efficiently. With $a_0 = 5$, corresponding to the intensity of $7 \times 10^{19}\,\mathrm{W\,cm^{-2}}$ and the power of 70 TW (with spot size diameter $16\lambda_L$), the obtainable proton quasi-monoenergy for 90% carbon and 10% hydrogen composite target can reach as high as 61 MeV, more than five times the energy obtainable from pure hydrogen targets.

We found in our previous work [42] that the effective accelerating time of the RPA on a single-ion foil is $14T_L$, nearly constant. The energy obtained from the RPA can then be estimated as 16.6MeV for a pure hydrogen foil and decreases to 5.0 MeV for a pure carbon foil due to increasing mass. For a carbon percentage lower than 50%, the total obtainable proton energy is about the same as the energy from the RPA, showing that high carbon ion concentration is a necessary condition for the SCR to take effect. A 1D theoretical model of the SCR phase is developed below in order to estimate the obtainable energy.

4. Theoretical model of the proton acceleration by shielded Coulomb repulsion

From the discussion above (see figure 3), we conclude that high carbon concentration helps to increase the obtainable proton energy through SCR. We would like to present here a theoretical

model for SCR of the protons by the carbon layer. We first derive the electric potential and the electric field of the electron-shielded carbon layer and then solve the equation of motion for the proton, as a test particle in the given field. We assume that the carbon and proton layers are completely separated, and protons are such a small minority with almost no effects on the carbon motion. We consider the electrostatic force on the proton layer (acting like a test particle) in a frame moving with the constant velocity v_C of the carbon layer. The terminal velocity is achieved due to the RPA phase, which is terminated when the electrons become almost transparent to the laser light. This is due to the RTI rendering the electron layer density ripple so large that the electron layer becomes underdense, and the radiation pressure can no longer hold the electrons. The electrons can move until they achieve the balance of the electric force and the thermal force due to their pressure, which is then of the order of radiation pressure, indicating their temperature being of the order of ponderomotive energy. The electron density, thus, has a Boltzmann distribution as electrons are very hot, and the electrostatic potential on the proton layer with electron screening is governed by the Poisson equation with Boltzmann electrons as a charge source,

$$\frac{\mathrm{d}^2\phi}{\mathrm{d}x^2} = \frac{en_0}{\varepsilon_0}\exp\left(\frac{e\phi}{k_\mathrm{B}T_\mathrm{e}}\right), \tag{2}$$

where the electric field boundary condition is determined by the net charge of carbon ions and electrons via Gauss's law. Multiplying equation (2) by $\mathrm{d}\phi/\mathrm{d}x$ and integrating along x, we have

$$\frac{1}{2}\left(\frac{\mathrm{d}\phi}{\mathrm{d}x}\right)^2 = \frac{n_0 k_\mathrm{B}T_\mathrm{e}}{\varepsilon_0}\left[\exp\left(\frac{e\phi}{k_\mathrm{B}T_\mathrm{e}}\right) + C_1\right]. \tag{3}$$

Integrating again, we then have

$$\phi\,(x) = \frac{2k_\mathrm{B}T_\mathrm{e}}{-e}\ln\left[\frac{1}{\sqrt{C_1}}\sinh\sqrt{\frac{C_1}{2}}\left(\frac{x}{\lambda_\mathrm{D}} + C_2\right)\right], \tag{4}$$

where C_1 and C_2 are integration constants, and $\lambda_\mathrm{D} = \sqrt{\varepsilon_0 k_\mathrm{B}T_\mathrm{e}/n_0 e^2}$ is the Debye length. Therefore the electric field can be derived from the electric potential as

$$E_x = -\frac{\mathrm{d}\phi}{\mathrm{d}x} = \frac{\sqrt{2C_1}k_\mathrm{B}T_\mathrm{e}}{e\lambda_\mathrm{D}}\coth\sqrt{\frac{C_1}{2}}\left(\frac{x}{\lambda_\mathrm{D}} + C_2\right). \tag{5}$$

The integration constant C_1 can be determined without knowing the detailed charge distribution by Gauss's law that $E_x = \sigma_\mathrm{net}/2\varepsilon_0$ when the position x is very far from the carbon layer, where $\sigma_\mathrm{net} = e\int(6n_\mathrm{C} - n_\mathrm{e})\mathrm{d}x$ is the net surface charge density of the carbon-electron foil. That is,

$$E_x \to \frac{\sqrt{2C_1}k_\mathrm{B}T_\mathrm{e}}{e\lambda_\mathrm{D}} = \frac{\sigma_\mathrm{net}}{2\varepsilon_0} \Rightarrow \sqrt{2C_1} = \frac{e\lambda_\mathrm{D}\sigma_\mathrm{net}}{2\varepsilon_0 k_\mathrm{B}T_\mathrm{e}}. \tag{6}$$

The whole system moves with velocity v_C, and hence the constant C_2, acting as a shift in x without altering the field profile, can be absorbed into the initial condition of the position. We can then express the equation of motion in the laboratory frame as

$$\begin{cases} \dfrac{\mathrm{d}x_\mathrm{p}}{\mathrm{d}t} = v_\mathrm{p}, \\ \dfrac{\mathrm{d}(\gamma_\mathrm{p}v_\mathrm{p})}{\mathrm{d}t} = \dfrac{eE_x}{m_\mathrm{p}} = \dfrac{e\sigma_\mathrm{net}}{2\varepsilon_0 m_\mathrm{p}}\coth\dfrac{\left(x_\mathrm{p} - v_\mathrm{C}t\right)e\sigma_\mathrm{net}}{4\varepsilon_0 k_\mathrm{B}T}. \end{cases} \tag{7}$$

The system of equations (7) can be solved numerically with the coefficients and initial conditions obtained from the simulation. The parameters and the results using a foil made of 90% carbon and 10% hydrogen are shown in figure 4. The initial time is chosen to be $t_0 = 50T_L$, the time of complete separation between the carbon ion layer and the proton layer as shown in figure 4(a). The initial displacement is determined by the initial acceleration, and the result $x_{p0} - v_C t_0 = 1.3\lambda_L$ is consistent with the density plot shown in figure 4(a), where the carbon layer velocity v_C, as shown in figure 2(a), is a constant $0.07c$, comparable to its sound speed. The evolution of the center of mass of the carbon layer as shown in figure 4(b), in comparison with the integrated value from its average velocity, verifies that the carbon-electron system moves with a constant velocity and hence the validity of describing the accelerating process in the inertial frame moving with such a velocity. The temperature of the Maxwell-distributed underdense electrons in the center-of-mass frame, as shown in figure 4(c), is kept roughly a constant $k_B T_e = 2.46 m_e c^2$ by the continuous laser wave. The agreement in the distribution between the simulation and the theory also verifies the validity of equation (2). The difference in charges during $50 < t/T_L < 150$ within the window $-1 < y/\lambda_L < 1$ is seen in figure 4(d), where we assume that the number of particles escaping this range that do not effectively participate in the acceleration scheme is 0.07 times the initial electrons on average. This is the main factor deciding the acceleration and is the reason why we call it SCR. One important consequence from this observation is that a large concentration of carbon is necessary for the initially less abundant positive charges of carbon ions to overcome the gradually escaping electrons after the end of the RPA phase. Although the acceleration is relatively small compared to the RPA, the accelerating time is much longer due to the negative slope in the electric field, which exerts a greater force on the protons left behind. The comparison between the theoretical calculation and the simulation result in figure 4(e) shows great consistency initially, and some deviation after the separation between the proton layer and the carbon ion layer is too large to use the 1D approximation. To increase the obtainable energy, we should either increase the input amplitude (larger T_e and v_C) or apply a larger number of carbon ions (larger σ_{net}), which could be achieved by increasing the carbon concentration (figure 3) or increasing the overall number of particles in the foil (discussed in the next section).

5. Further boosting of energy by increasing the initial foil density and the input laser intensity

From the argument above, we can see that the acceleration and obtainable energy depend more on SCR with a higher carbon ion concentration. The acceleration due to SCR is proportional to the number of positive charges behind the protons. Increasing the initial density seems to be a promising way of increasing the obtainable energy. As long as the carbon and proton layers are separated during the RPA phase, increasing the initial density can enhance not only the acceleration but also the number of protons.

To verify this statement, we carried out a series of simulations with the same parameters as mentioned in the previous section but setting the initial density three times as large. The result is shown in figure 5. We first note that the threshold for the enhancement in SCR to compensate for the reduction of the RPA is still around 50%, which gives an empirical general criterion in this acceleration scheme. Second, the acceleration time is significantly enhanced, especially in the cases of 80% and 90% carbon concentrations, which implies that the acceleration by SCR is very stable for high initial carbon concentration.

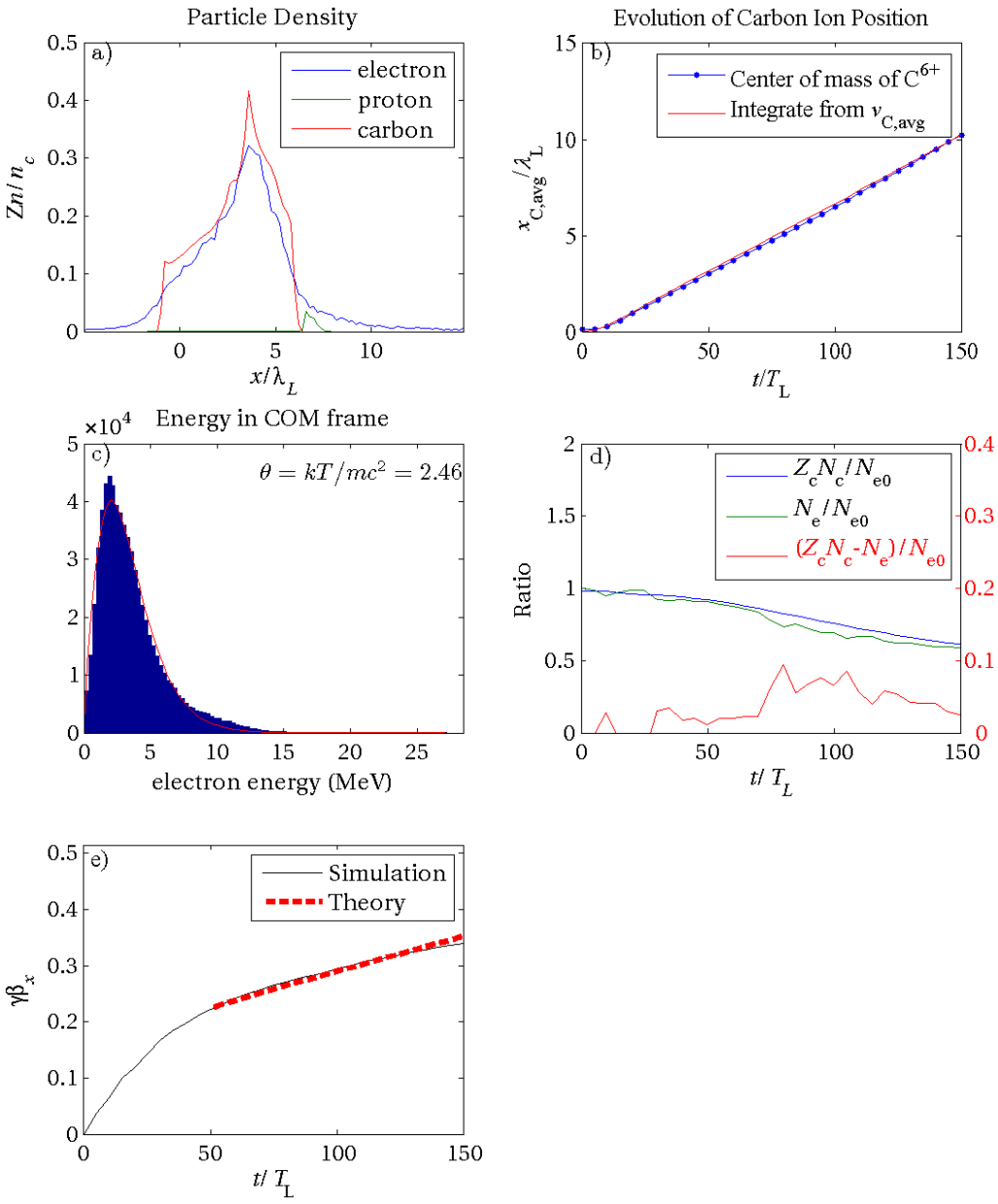

Figure 4. Simulation and theoretical results using a foil made of 90% carbon and 10% hydrogen: (a) the initial particle densities around the proton position $x_0 = 2.5\lambda_L$, (b) the center of carbon ion layer, (c) the electron energy distribution in the center-of-mass frame, compared to a Maxwellian distribution with temperature $k_B T_e/m_e c^2 = 2.46$, (d) the relative particle densities in the foil, showing that the total relative particle charge is $\sigma_{net}/\sigma_e 0 = 0.07$, and (e) a comparison between the proton energy obtained in the simulation (solid line) and the theoretical SCR model (dashed line). The initial velocity $\gamma\beta_{x0} = 0.022$ is used in the theoretical calculation.

In figure 6, we show the case with higher intensity $a_0 = 10$, which corresponds to 270 TW power. It shows that 100 MeV monoenergy protons could be achieved with multi-ion foils, whereas with a single-ion foil it can reach a monoenergy of merely 50 MeV [42]. The result

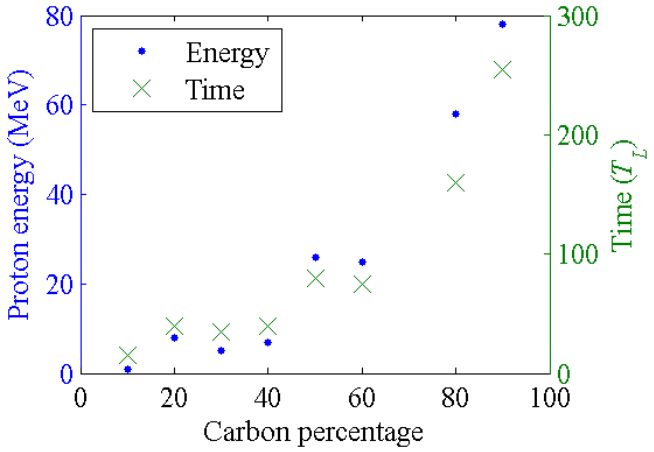

Figure 5. Similar plot as in figure 3 but with three times as large initial foil densities.

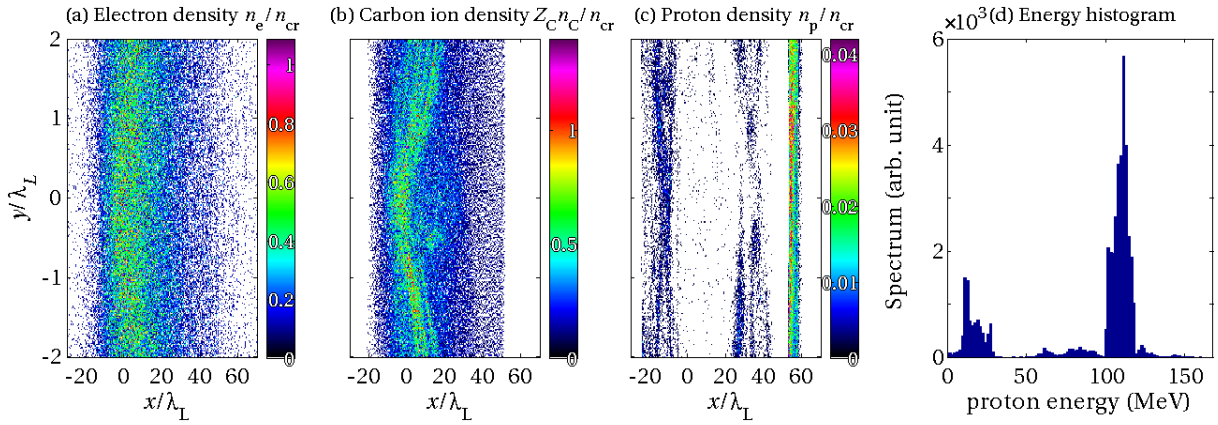

Figure 6. The simulation result at $t = 190T_L$ with input parameters the same as in figure 1, except for $a_0 = 10$, $n_{e0} = 100n_{cr}$ and $n_C : n_p = 9 : 1$, showing the number densities of (a) electrons, (b) carbon ions and (c) protons. Panel (d) shows the proton energy histogram within a window of $|y| < \lambda_L$, covering the entire simulation range in x.

in figure 6 shows that the monoenergetic peak at $t = 190T_L$ with energy 110 MeV is sharp ($\Delta\mathcal{E}/\mathcal{E} = 7\%$), omitting the low-energy peak due to the protons moving backwards.

6. The effects of a smaller spot size

The evolution of energy in the 1D theoretical model discussed in section 5 fits well if the charge distribution in the central part is independent of the perpendicular dimension y. This assumption fails far away from the foil if a smaller laser spot size of $2\lambda_L$ instead of $16\lambda_L$ is used. However, even though the acceleration value calculated in the 1D model does not match the 2D simulation value, the mechanism for SCR is the same. The density distribution in figure 7 shows that only the particles in the vicinity of the central axis are affected, and the protons from the central part

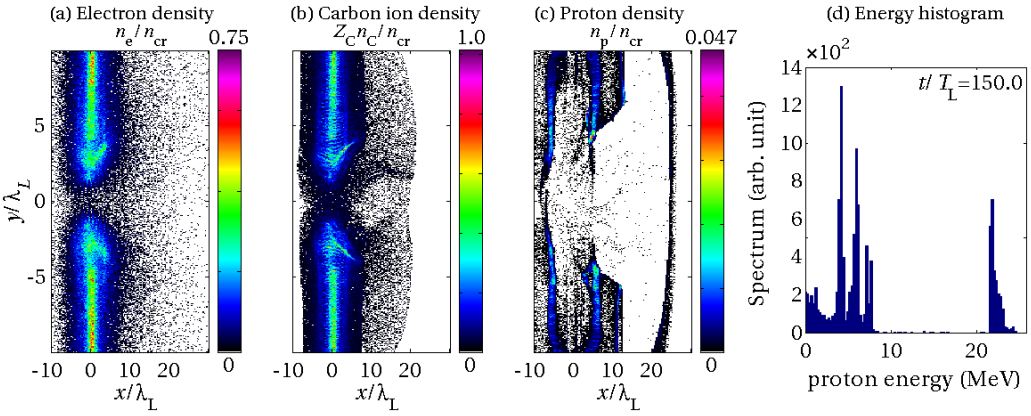

Figure 7. The simulation result at $t = 150T_L$ with input parameters the same as in figure 1, except for the spot size being $2\lambda_L$ in diameter, showing the number densities of (a) electrons, (b) carbon ions and (c) protons. Panel (d) shows the proton energy histogram within a window of $|y| < \lambda_L$, covering the entire simulation range in x.

then expands largely in the y-direction. Immobility of carbon ions in the large-y region results in less effective acceleration; as shown in figure 7(d) only 22 MeV of proton beam, corresponding to $\gamma\beta_x = 0.22$, is obtained. Greater expansion of protons in the y-direction largely reduces the total number of protons in the quasi-monoenergetic peak to 1.7×10^6, about 1/30 of the value obtained with the original parameters, which is 5.5×10^7. However, since the input power of the laser beam due to a smaller spot size is also reduced to 1/64 (1.1 TW in value), the portion of laser energy converted to the quasi-monoenergetic protons is 90% of the value with large spot size. Therefore, this acceleration scheme could, in principle, be applied to cases with more realistic settings as well.

7. Conclusions

In summary, we have compared the laser acceleration of single- and multi-ion foils and found energy scaling for different ion concentrations. The detrimental effects of the RTI of pure hydrogen foils are significantly reduced by the inclusion of carbon ions, which give an additional boost to the proton energy via SCR. With increasing the carbon concentration, the acceleration time is significantly extended, and consequently the obtainable monoenergy is also considerably increased. In particular, we found that there exists a critical value of carbon concentration above which the SCR is effective due to a distinct separation between the two different ion species. The proton monoenergy can be further boosted with a denser foil due to a greater repulsive force from the carbon ions. The resulting proton monoenergy could reach 78 MeV by using a laser beam of merely 70 TW, a significant reduction in the required laser power. Moreover, 110 MeV of proton energy can also be obtained by a laser beam of input power 270 TW, which is a promising result for future applications.

Acknowledgments

This work was supported by US DoE grant DE-SC0008391. We would like to acknowledge the National Center for High-Performance Computing in providing resources under the national project 'Taiwan Knowledge Innovation National Grid'. We also appreciate helpful discussions with Professor R Sagdeev, K Papadopoulos and G Dudnikova.

Appendix. Theoretical model of radiation pressure acceleration

In RPA, a high-intensity circularly polarized laser with a high contrast ratio accelerates the ultra-thin foil by the ponderomotive force acting on the electrons. The resulting space-charge electric field pulls the ions and makes the foil accelerate as a whole. The equation of motion for the foil in one dimension, based on energy conservation [21, 25, 30, 31, 49, 50], is

$$\frac{\mathrm{d}(\gamma\beta)}{\mathrm{d}t} = \frac{2I_0}{Mc^2}\frac{1-\beta}{1+\beta}, \tag{A.1}$$

where $\gamma = (1-\beta^2)^{-1/2}$ is the relativistic gamma factor, $\beta = v/c$ is the normalized foil velocity, $M = m_\mathrm{i} n_\mathrm{i0} l_0$ is the mass density of the ion layer, m_i is the ion mass, n_i0 is the ion number density, l_0 is the foil thickness, $I_0 = \varepsilon_0(E_y^2 + E_z^2)c$ is the laser intensity, E_y and E_z are the y and z components of the laser electric field, ε_0 is the electric permittivity in vacuum and c is the speed of light in vacuum. Equation (A.1) can be analytically solved as [26]

$$\gamma\beta = \frac{\psi^2 - 1}{2\psi}, \tag{A.2}$$

where

$$\psi = 2\sinh\left\{\frac{1}{3}\sinh^{-1}\left[2 + 6\frac{m_\mathrm{e}}{m_\mathrm{i}}\frac{n_\mathrm{cr}}{n_\mathrm{i0}}\frac{\lambda_\mathrm{L}}{l_0}\int_0^t \left(a_y^2 + a_z^2\right)\frac{\mathrm{d}s}{T_\mathrm{L}}\right]\right\}, \tag{A.3}$$

from which the ion kinetic energy $\mathcal{E}_\mathrm{i}(t) = (\gamma - 1)m_\mathrm{i}c^2$ and momentum $p_{\mathrm{i}x} = \gamma\beta m_\mathrm{i} c$ are obtained. Here m_e is the electron mass, $n_\mathrm{cr} = \varepsilon_0 m_\mathrm{e}\omega_\mathrm{L}^2/e^2$ is the critical density, $a_y = eE_y/m_\mathrm{e}c\omega_\mathrm{L}$ and $a_z = eE_z/m_\mathrm{e}c\omega_\mathrm{L}$ are the y and z components of the normalized laser amplitude, and λ_L, ω_L and T_L are the laser wavelength, angular frequency and period, respectively. Due to the large-amplitude laser beam, the foil is fully ionized and is in a plasma state. In a 1D geometry using a circularly polarized laser beam [25–27], the electrons are trapped in a well, pushed by the laser ponderomotive force from one side of the foil and pulled pack by the ion electric field from the other side of the foil. A majority of the ions are also stably trapped by the combined inertial force and electric field, which constitute a potential well for the ions in the accelerated frame of the foil [25, 27]. By necessity, a fraction of the ions are untrapped and are left behind the accelerated foil. The space-charge electric field between these ions and the electrons keeps the rest of the ions trapped in the foil. Through a balance between the electric force and the inertial force in the accelerated frame, the fraction of untrapped ions can be estimated as [27] $N_\mathrm{untrapped}/N_0 = 2\varepsilon_0 I_0/N_0^2 e^2 c$, where $N_0 = n_\mathrm{i0} l_0$ is the total surface number density of ions. With linearly polarized light, the electrons are strongly heated and the foil quickly fractures due to thermal expansion and the RPA is inefficient [26]. In multiple dimensions, the time for monoenergetic ion acceleration with RPA is limited by the development of the

RTI [24, 26, 38–41] to about $16T_L$ [42] for a proton foil. In this case a majority species of heavy ions can be employed to set up a space-charge electric field to efficiently accelerate a population of protons via the SCR process, as described in this paper.

References

[1] Wilson R R 1946 Radiological use of fast protons *Radiology* **47** 487–91
[2] Jones B 2005 Radiotherapy for the future *BMJ* **330** 979–80
[3] Jones B 2006 The case for particle therapy *Br. J. Radiol.* **79** 24–31
[4] Ledingham K 2006 Desktop accelerators: going up? *Nature Phys.* **2** 11–2
[5] Ledingham K W D, Galster W and Sauerbrey R 2007 Laser-driven proton oncology—a unique new cancer therapy? *Br. J. Radiol.* **80** 855–8
[6] Geddes C G R, Toth C, van Tilborg J, Esarey E, Schroeder C B, Bruhwiler D, Nieter C, Cary J and Leemans W P 2004 High-quality electron beams from a laser wakefield accelerator using plasma-channel guiding *Nature* **431** 538–41
[7] Mangles S P D *et al* 2004 Monoenergetic beams of relativistic electrons from intense laser–plasma interactions *Nature* **431** 535–8
[8] Faure J, Glinec Y, Pukhov A, Kiselev S, Gordienko S, Lefebvre E, Rousseau J-P, Burgy F and Malka V 2004 A laser–plasma accelerator producing monoenergetic electron beams *Nature* **431** 541–4
[9] Tajima T and Dawson J M 1979 Laser electron accelerator *Phys. Rev. Lett.* **43** 267–70
[10] Leemans W P, Nagler B, Gonsalves A J, Toth C, Nakamura K, Geddes C G R, Esarey E, Schroeder C B and Hooker S M 2006 GeV electron beams from a centimetre-scale accelerator *Nature Phys.* **2** 696–9
[11] Kneip S *et al* 2009 Near-GeV acceleration of electrons by a nonlinear plasma wave driven by a self-guided laser pulse *Phys. Rev. Lett.* **103** 035002
[12] Wilks S C, Langdon A B, Cowan T E, Roth M, Singh M, Hatchett S, Key M H, Pennington D, MacKinnon A and Snavely R A 2001 Energetic proton generation in ultra-intense laser–solid interactions *Phys. Plasmas* **8** 542–9
[13] Pukhov A 2001 Three-dimensional simulations of ion acceleration from a foil irradiated by a short-pulse laser *Phys. Rev. Lett.* **86** 3562–5
[14] Schwoerer H, Pfotenhauer S, Jackel O, Amthor K-U, Liesfeld B, Ziegler W, Sauerbrey R, Ledingham K W D and Esirkepov T 2006 Laser–plasma acceleration of quasi-monoenergetic protons from microstructured targets *Nature* **439** 445–8
[15] Hegelich B M, Albright B J, Cobble J, Flippo K, Letzring S, Paffett M, Ruhl H, Schreiber J, Schulze R K and Fernández J C 2006 Laser acceleration of quasi-monoenergetic MeV ion beams *Nature* **439** 441–4
[16] Ter-Avetisyan S, Schnürer M, Nickles P V, Kalashnikov M, Risse E, Sokollik T, Sandner W, Andreev A and Tikhonchuk V 2006 Quasimonoenergetic deuteron bursts produced by ultraintense laser pulses *Phys. Rev. Lett.* **96** 145006
[17] Fuchs J *et al* 2006 Laser-driven proton scaling laws and new paths towards energy increase *Nature Phys.* **2** 48–54
[18] Mora P 2007 Laser driven ion acceleration *AIP Conf. Proc.* **920** 98–117
[19] Yin L, Albright B J, Hegelich B M, Bowers K J, Flippo K A, Kwan T J T and Fernández J C 2007 Monoenergetic and GeV ion acceleration from the laser breakout afterburner using ultrathin targets *Phys. Plasmas* **14** 056706
[20] Robson L *et al* 2007 Scaling of proton acceleration driven by petawatt-laser-plasma interactions *Nature Phys.* **3** 58–62
[21] Esirkepov T, Borghesi M, Bulanov S V, Mourou G and Tajima T 2004 Highly efficient relativistic-ion generation in the laser-piston regime *Phys. Rev. Lett.* **92** 175003
[22] Yan X Q, Lin C, Sheng Z M, Guo Z Y, Liu B C, Lu Y R, Fang J X and Chen J E 2008 Generating high-current monoenergetic proton beams by a circularly polarized laser pulse in the phase-stable acceleration regime *Phys. Rev. Lett.* **100** 135003

[23] Liu C S, Tripathi V K and Shao X 2008 *Laser Acceleration of Monoenergetic Protons Trapped in Moving Double Layer* (*AIP Conf. Proc.* 1061) ed P K Shukla, B Eliasson and L Stenflo (New York: AIP) pp 246–54
[24] Klimo O, Psikal J, Limpouch J and Tikhonchuk V T 2008 Monoenergetic ion beams from ultrathin foils irradiated by ultrahigh-contrast circularly polarized laser pulses *Phys. Rev. ST Accel. Beams* **11** 031301
[25] Tripathi V K, Liu C S, Shao X, Eliasson B and Sagdeev R Z 2009 Laser acceleration of monoenergetic protons in a self-organized double layer from thin foil *Plasma Phys. Control. Fusion* **51** 024014
[26] Robinson A P L, Zepf M, Kar S, Evans R G and Bellei C 2008 Radiation pressure acceleration of thin foils with circularly polarized laser pulses *New J. Phys.* **10** 013021
[27] Eliasson B, Liu C S, Shao X, Sagdeev R Z and Shukla P K 2009 Laser acceleration of monoenergetic protons via a double layer emerging from an ultra-thin foil *New J. Phys.* **11** 073006
[28] Henig A *et al* 2009 Radiation-pressure acceleration of ion beams driven by circularly polarized laser pulses *Phys. Rev. Lett.* **103** 245003
[29] Jung D *et al* 2011 Monoenergetic ion beam generation by driving ion solitary waves with circularly polarized laser light *Phys. Rev. Lett.* **107** 115002
[30] Marx G 1966 Interstellar vehicle propelled by terrestrial laser beam *Nature* **211** 22–3
[31] Simmons J F L and McInnes C R 1993 Was Marx right? Or how efficient are laser driven interstellar spacecraft? *Am. J. Phys.* **61** 205
[32] He M-Q, Dong Q-L, Sheng Z-M, Weng S-M, Chen M, Wu H-C and Zhang J 2007 Acceleration dynamics of ions in shocks and solitary waves driven by intense laser pulses *Phys. Rev.* E **76** 035402(R)
[33] Palmer C A J *et al* 2011 Monoenergetic proton beams accelerated by a radiation pressure driven shock *Phys. Rev. Lett.* **106** 014801
[34] Haberberger D, Tochitsky S, Fiuza F, Gong C, Fonseca R A, Silva L O, Mori W B and Joshi C 2011 Collisionless shocks in laser-produced plasma generate monoenergetic high-energy proton beams *Nature Phys.* **8** 95–9
[35] He M-Q, Shao X, Liu C-S, Liu T-C, Su J-J, Dudnikova G, Sagdeev R Z and Sheng Z-M 2012 Quasi-monoenergetic protons accelerated by laser radiation pressure and shocks in thin gaseous targets *Phys. Plasmas* **19** 073116
[36] Macchi A, Cattani F, Liseykina T V and Cornolti F 2005 Laser acceleration of ion bunches at the front surface of overdense plasmas *Phys. Rev. Lett.* **94** 165003
[37] Qiao B, Zepf M, Borghesi M and Geissler M 2009 Stable GeV ion-beam acceleration from thin foils by circularly polarized laser pulses *Phys. Rev. Lett.* **102** 145002
[38] Snavely R A *et al* 2000 Intense high-energy proton beams from petawatt-laser irradiation of solids *Phys. Rev. Lett.* **85** 2945–8
[39] Pegoraro F and Bulanov S V 2007 Photon bubbles and ion acceleration in a plasma dominated by the radiation pressure of an electromagnetic pulse *Phys. Rev. Lett.* **99** 065002
[40] Liu C S *et al* 2012 Laser radiation pressure accelerator for quasi-monoenergetic proton generation and its medical implications *Progress in Ultrafast Intense Laser Science VIII* (*Springer Series in Chemical Physics* vol 103) ed K Yamanouchi, M Nisoli, W T Hill, A W Castleman, J P Toennies, K Yamanouchi and W Zinth (Berlin: Springer) pp 177–95
[41] Palmer C 2012 Rayleigh–Taylor instability of an ultrathin foil accelerated by the radiation pressure of an intense laser *Phys. Rev. Lett.* **108** 225002
[42] Liu T-C, Shao X, Liu C-S, Su J-J, Eliasson B, Tripathi V, Dudnikova G and Sagdeev R Z 2011 Energetics and energy scaling of quasi-monoenergetic protons in laser radiation pressure acceleration *Phys. Plasmas* **18** 123105
[43] Chen M, Pukhov A, Yu T P and Sheng Z M 2009 Enhanced collimated GeV monoenergetic ion acceleration from a shaped foil target irradiated by a circularly polarized laser pulse *Phys. Rev. Lett.* **103** 024801
[44] Yu T-P, Pukhov A, Shvets G and Chen M 2010 Stable laser-driven proton beam acceleration from a two-ion-species ultrathin foil *Phys. Rev. Lett.* **105** 065002
[45] Yu T P, Pukhov A, Shvets G, Chen M, Ratliff T H, Yi S A and Khudik V 2011 Simulations of stable compact proton beam acceleration from a two-ion-species ultrathin foil *Phys. Plasmas* **18** 043110

[46] Bulanov S S *et al* 2008 Accelerating monoenergetic protons from ultrathin foils by flat-top laser pulses in the directed-Coulomb-explosion regime *Phys. Rev.* E **78** 026412
[47] Pae K H, Choi I W and Lee J 2011 Effect of target composition on proton acceleration by intense laser pulses in the radiation pressure acceleration regime *Laser Part. Beams* **29** 11–6
[48] Qiao B, Zepf M, Borghesi M, Dromey B, Geissler M, Karmakar A and Gibbon P 2010 Radiation-pressure acceleration of ion beams from nanofoil targets: the leaky light-sail regime *Phys. Rev. Lett.* **105** 155002
[49] Einstein A 1905 Zur Elektrodynamik bewegter Körper *Ann. Phys. Lpz.* **17** 891–921
[50] Censor D 1971 Energy balance and radiation forces for arbitrary moving objects *Radio Sci.* **6** 903–10